Glycine Valence Orbital Electron Densities: Comparison of Electron Momentum Spectroscopy Experiments with Hartree−Fock and Density Functional Theories

John J. Neville, Y. Zheng, and C. E. Brion*

Contribution from the Department of Chemistry, University of British Columbia, 2036 Main Mall, Vancouver, British Columbia, Canada V6T 1Z1

Received April 22, 1996[⊗]

Abstract: Experimental momentum profiles (orbital images) corresponding to the electron density distribution in the outer valence shell of gaseous glycine have been obtained by electron momentum spectroscopy measurements conducted over the binding energy range of 6−27 eV at an impact energy of 1200 eV + binding energy. The experimental data are compared with theoretical momentum profiles calculated using Hartree−Fock and Kohn−Sham density functional theories. The calculated momentum profiles correspond to a Boltzmann weighted sum of the five dominant conformers predicted to be present at the experimental temperature of 165 °C. The importance of basis set size and flexibility is investigated in the case of the Hartree−Fock results by performing calculations using a series of basis sets ranging from minimal (STO-3G) to the near-Hartree−Fock limit (aug-cc-pVTZ). The sensitivity of the density functional theory calculations to the type of exchange-correlation potential energy functional is investigated by comparing results using the local density approximation with those obtained with nonlocal functionals proposed by Becke, Perdew, and Lee, Yang, and Parr. It is found that the experimental results are generally best modeled by the density functional theory calculations, with only small differences noted among the results obtained using the different potential energy functionals. In the case of the Hartree−Fock calculations, increasing the basis set size beyond that of the 6-311++G** basis set has no discernible effect on the calculated momentum profiles, which in comparison to the experimental momentum profiles tend to underestimate the intensity at low values of electron momentum, particularly for the outermost valence orbitals of glycine. This suggests that a consideration of electron correlation effects is necessary for correct modeling of the chemically sensitive outer spatial regions of the electron density of the outer valence orbitals of glycine.

Introduction

A detailed understanding of the electronic structure and orbital electron density distribution in biomolecules such as amino acids is of considerable interest and importance from a fundamental standpoint. Such information is relevant to applications in protein biochemistry and medicinal chemistry and also necessary to provide meaningful input for computer-aided molecular design and reactivity studies. In particular, a detailed knowledge of the electron density distributions and motion of electrons in the frontier orbitals is required to understand and model the tendency for reactivity and structural concepts such as intramolecular hydrogen bonding.[1] For many problems involving molecular recognition and reactivity the long-range (i.e., outer spatial) region of the frontier orbital electron density is an important consideration.[2−4] However, it has been shown[5−9] that even in some simple molecules such as H_2O and NH_3 the electron density in such regions is often not well modeled in quantum mechanical calculations unless very large saturated and diffuse basis sets and correlated treatments such as multireference single and double configuration interaction (MRSD-CI) or density functional theory (DFT) are used.

The above theoretical conclusions have been strongly guided by experimental results obtained for the frontier orbitals of small hydrides[5−11] using electron momentum spectroscopy (EMS). EMS is an experimental technique [7,12] capable of imaging the electron density of binding energy selected electrons (i.e., effectively imaging the electron density of individual atomic and molecular orbitals). This experimental "orbital imaging" is in momentum space rather than the more familiar position space. EMS is most sensitive to regions of low momentum which strongly emphasize the chemically sensitive outermost spatial regions of electron density because of the Fourier transform relationship between momentum and position space. Although the outermost (large r) region of electron density plays a significant role in chemical reactivity, this area is often represented poorly by variationally determined wave functions as a result of its small contribution to the total energy, a property dominated by the core (small r) electron density. To ensure that a wave function accurately models all regions of electron density, it is important to consider a range of properties that

[⊗] Abstract published in *Advance ACS Abstracts,* October 1, 1996.

(1) Davidson, E. R. *Can. J. Phys*., in press.
(2) Measures, P. T.; Mort, K. A.; Allen, N. L.; Cooper, D. L. J. *Comput.-Aided Mol. Des*. **1995**, *9*, 331−340.
(3) Allan, N. L.; Cooper, D. L. *Top. Curr. Chem*. **1995**, *173*, 85−111.
(4) Cooper, D. L.; Allan, N. L. *J. Am. Chem. Soc*. **1992**, *114*, 4773−4776.
(5) Bawagan, A. O.; Brion, C. E.; Davidson, E. R.; Feller, D. *Chem. Phys.* **1987**, *113*, 19−42.
(6) Bawagan, A. O.; Müller-Fiedler, R.; Brion, C. E.; Davidson, E. R.; Boyle, C. *Chem. Phys.* **1988**, *120*, 335−337.
(7) Brion, C. E. In *The Physics of Electronic and Atomic Collisions*; Andersen, T., Fastrup, B., Folkmann, F., Knudsen, H., Andersen, N., Eds.; American Institute of Physics: New York, 1993; Vol. 295, pp 350−359 and references therein.
(8) Feller, D.; Boyle, C. M.; Davidson, E. R. *J. Chem. Phys*. **1987**, *86*, 3424−3440.
(9) Duffy, P.; Chong, D. P.; Casida, M. E.; Salahub, D. R. *Phys. Rev. A* **1994**, *50*, 4707−4728.
(10) French, C. L.; Brion, C. E.; Davidson, E. R. *Chem. Phys.* **1988**, *122*, 247−269.
(11) Clark, S. A. C.; Brion, C. E.; Davidson, E. R.; Boyle, C. *Chem. Phys*. **1989**, *136*, 55−66.
(12) McCarthy, I.; Weigold, E. *Rep. Prog. Phys*. **1991**, *91*, 789−879.

S0002-7863(96)01301-7 CCC: $12.00

each emphasizes a different region of space. The total energy (small r), dipole moment (medium r), and EMS momentum profiles (large r) have proven to be effective choices to guide the development of "universal" wave functions.[5,7,8] The fact that the low momentum (large r) regions of EMS momentum profile measurements are particularly sensitive to the role of electron correlation effects has been clearly demonstrated in the experimental and theoretical momentum space studies of the highest occupied molecular orbitals (HOMOs) of H_2O and NH_3.[5−7] The usefulness of working in momentum space when considering chemical reactivity has also been recently demonstrated in theoretical work by Allan, Cooper, and co-workers, who have found that molecular similarity indices calculated using momentum space electron densities are capable of rationalizing physical and chemical properties and biological activity in cases where analyses using position space electron densities are not definitive.[2,3,13] For example, such theoretical momentum space studies have been able to predict satisfactorily the relative effectiveness of anti-HIV phospholipids observed in clinical testing.[2,3,13]

To date, most EMS studies of orbital densities (momentum distributions) have been made on small molecules which are either gases or volatile liquids at room temperature. The extension of EMS measurements and the complementary quantum mechanical calculations to larger molecular systems such as amino acids poses a number of challenging problems both experimentally and theoretically. Experimental difficulties encountered with larger molecules include decreased data accumulation rates and, in most cases, much more closely spaced orbital (binding) energies and the lower sample volatility frequently associated with liquids and solids of higher molecular weight. These difficulties have been significantly reduced by improvements in instrumentation. Recently reported multichannel EMS spectrometers[14−16] have substantially improved the sensitivity over that of earlier single channel instruments.[17] The increased coincidence count rates (∼20 times, with significant further improvements possible) have also permitted a somewhat improved energy resolution to be employed. The development of a solid sample heated reservoir probe[18] has enabled the stable sublimation of low vapor pressure solid samples into the EMS collision region over long periods of time. These improvements have been demonstrated in a recent study of the valence electron density of acetone[15] and in preliminary reports[18,19] of the HOMO electron densities of dimethoxymethane and glycine. From a theoretical standpoint, computational complexity rapidly increases with molecular weight even at the Hartree−Fock (HF) level, and high-level correlated treatments such as configuration interaction (CI) quickly become unfeasible for larger molecules. The conformational mobility of many larger molecules further increases the computational difficulties since separate calculations of orbital electron density are required for each stable conformer (potential energy minimum) present under the particular experimental conditions. The individual conformer calculations must then be Boltzmann weighted at the experimental temperature and summed together prior to comparison with the EMS experimental data. DFT is now offering a computationally less intensive approach to quantum mechanical calculations with inclusion of electron correlation effects via the exchange-correlation potential. It is also noteworthy that DFT has satisfactorily reproduced high-level MRSD-CI calculations in comparisons with EMS measurements for small[9,20,21] and intermediate size[15] molecules and thus may provide a viable approach to the theoretical investigation of the role of electron correlation effects in the valence orbital densities of larger molecules.

The above advances have been used in the present work to facilitate a detailed and comprehensive experimental and theoretical investigation of the outer valence orbital electron density distributions of the simplest amino acid glycine (NH_2-CH_2COOH), which is of fundamental biological interest as well as being a prototype for larger systems. The roles of basis set size and composition and also electron correlation effects in modeling the outer valence orbitals of this molecule have been studied by comparing the experimental measurements to HF and DFT calculations using a range of basis sets.

The molecular structure of glycine has been the subject of considerable recent theoretical work. The conformational flexibility of the neutral glycine molecule, the form found in the gas phase, results in several stable conformers, considerably increasing the challenge of accurate theoretical modeling. Much of the theoretical work on glycine to date has focused on determining the geometries and relative energies of these stable conformers. It is apparent from this quantum mechanical work that the results for glycine are very sensitive to the theoretical method employed and to the nature of the basis set used. In particular, it has been found that the results from semiempirical and HF calculations vary considerably.[22] Conclusions based on HF calculations regarding the geometries and relative energies of the glycine conformers that are energy minima on the glycine potential energy surface are strongly basis set dependent.[22−24] The use of flexible basis sets containing both diffuse and polarization functions appears necessary in performing meaningful geometry optimization calculations on glycine, likely due to the presence of several nonbonding electron pairs and intramolecular hydrogen bonds.[24] Electron correlation effects have also been shown to play a significant role in glycine, with their inclusion, whether through Møller−Plesset (MP) perturbation theory,[24−26] CI,[27] or DFT,[28,29] having a particularly significant effect on the relative conformer energies. With respect to determining geometries, there is some disagreement as to the necessity of employing theoretical methods that take

(13) Cooper, D. L.; Mort, K. A.; Allan, N. L.; Kinchington, D.; McGuigan, C. *J. Am. Chem. Soc.* **1993**, *115*, 12615−12616.
(14) Weigold, E.; Zheng, Y.; von Niessen, W. *Chem. Phys.* **1991**, *150*, 405−427.
(15) Zheng, Y.; Neville, J. J.; Brion, C. E.; Wang, Y.; Davidson, E. R. *Chem. Phys.* **1994**, *188*, 109−129.
(16) Todd, B. R.; Lermer, N.; Brion, C. E. *Rev. Sci. Instrum.* **1994**, *65*, 349−358.
(17) See ref 15 and 18 for comparisons of experimental data obtained using single channel and multichannel spectrometers.
(18) Neville, J. J.; Zheng, Y.; Hollebone, B. P.; Cann, N.; Brion, C. E.; Kim, C.-K.; Wolfe, S. *Can. J. Phys.*, in press.
(19) Zheng, Y.; Neville, J. J.; Brion, C. E. *Science* **1995**, *270*, 786−788.
(20) Hollebone, B. P.; Neville, J. J.; Zheng, Y.; Brion, C. E.; Wang, Y.; Davidson, E. R. *Chem. Phys.* **1995**, *196*, 13−35.
(21) Duffy, P. A Combined Experimental and Theoretical Study of the Electronic Structure of Molecules by Electron Momentum Spectroscopy and Density Functional Theory. Ph.D. Thesis, University of British Columbia, 1995.
(22) Jensen, J. H.; Gordon, M. S. *J. Am. Chem. Soc.* **1991**, *113*, 7917−7924.
(23) Ramek, M.; Cheng, V. K. W.; Frey, R. F.; Newton, S. Q.; Schäfer, L. *J. Mol. Struct.* **1991**, *235*, 1−10.
(24) Yu, D.; Armstrong, D. A.; Rauk, A. *Can. J. Chem.* **1992**, *70*, 1762−1772.
(25) Császár, A. G. *J. Am. Chem. Soc.* **1992**, *114*, 9568−9575.
(26) Frey, R. F.; Coffin, J.; Newton, S. Q.; Ramek, M.; Cheng, V. K. W.; Momany, F. A.; Schäfer, L. *J. Am. Chem. Soc.* **1992**, *114*, 5369−5377.
(27) Hu, C.-H.; Shen, M.; Schaefer, H. F., III. *J. Am. Chem. Soc.* **1993**, *115*, 2923−2929.
(28) Barone, V.; Adamo, C.; Lelj, F. *J. Chem. Phys.* **1995**, *102*, 364−370.
(29) Nguyen, D. T.; Scheiner, A. C.; Andzelm, J. W.; Sirois, S.; Salahub, D. R.; Hagler, A. T. Submitted for publication to *J. Am. Chem. Soc.*

account of electron correlation effects in glycine.[26,30,31] Regardless, recent high-level calculations using large basis sets and MP2,[25] CI,[27] and DFT including the HF exchange energy[28,29] are in fairly close agreement not only for the conformer geometries but also for their relative energies.

The need to perform relatively large calculations in order to obtain dependable results for the geometries and relative energies of glycine conformers raises the question as to the sensitivity of other calculated properties of glycine to basis set size and composition and to electron correlation effects. Because of the importance of the outer valence orbitals and in particular the HOMO electron density to chemical reactivity,[32,33] it is of particular interest to investigate the importance of the considerations mentioned above to the valence orbital electron density distributions in glycine. As noted above, EMS measurements and associated calculations have clearly shown that electron correlation effects are a determining factor in the long-range (low momentum) parts of the outer valence orbital electron density distributions in NH_3[6,7] and the methylamines.[34] Therefore, since for most conformers of glycine the HOMO electron density is predominantly located on the nitrogen atom, it is of interest to see if similar electron correlation effects are also a determining factor in the valence orbital electron density distributions of glycine.

Several other previously published studies are pertinent to the current work. The outer valence photoelectron spectrum of glycine has been reported by Debies and Rabalais[35] in 1974 and by Cannington and Ham[36] in 1983 using He(I) and He(II) resonance radiation, respectively. Both studies found three peaks in the low binding energy region, at 10.0, 11.1, and 12.1 eV, assigned as ionizations from nonbonding nitrogen (HOMO), carbonyl oxygen, and hydroxyl oxygen orbitals, respectively. The two studies made the same assignments for the symmetry of the second and third orbitals (a′ and a″ respectively) but differed on the symmetry of the HOMO, with Debies and Rabalais predicting an out-of-plane (a″) orbital and Cannington and Ham predicting an in-plane (a′) orbital.

As stated above, there are several stable conformers of glycine present in the gas phase. In fact, theoretical studies have found as many as eight conformers[22−25,27,28] (see Figure 1 and ref 37). However, only a few of these conformers have been observed experimentally. Both conformers **Ip** and **IIp** have been identified by microwave spectroscopy.[38−42] In the recent study by Godfrey and Brown,[42] the nonobservance of conformers other than **Ip** and **IIp**, in combination with a consideration of their instrumental sensitivity and estimated absorption coefficients for conformers **IIp** and **IIIp**, initially led to the prediction of an upper limit of 0.2 for the abundance of **IIIp** relative to that of **IIp** at the experimental temperature of 235 °C. In contrast, the most elaborate theoretical studies[25,27,28] predict that conformer **IIIp** should be present in a proportion considerably larger than this. In this regard, Godfrey and Brown[42] point out that their limited observations (only **Ip** and **IIp**) could be due to relaxation of the other conformers to **Ip** in the expanding gas jet. A recently published theoretical study[43] of the barriers to interconversion between glycine conformers indicates that this explanation is likely correct. This is further supported by recently reported evidence for a third conformer, obtained by an infrared spectroscopy study of glycine trapped in inert gas matrices.[44]

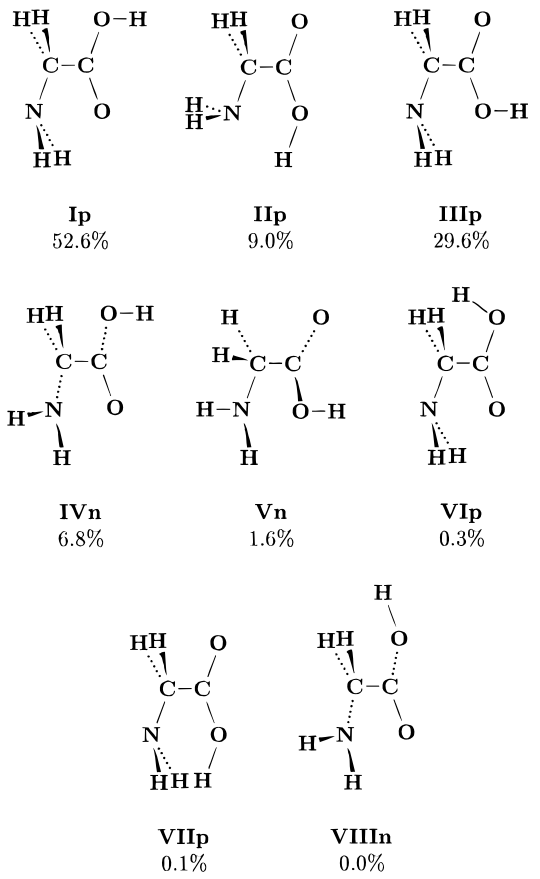

Figure 1. Conformers predicted to be energy minima on the glycine potential energy surface.[25] Following the labeling scheme used in ref 25, **p** denotes a C_s symmetry conformer and **n** a C_1 symmetry conformer. The calculated abundance of each conformer based on the relative free energies (see the Theoretical Methods and Table 2) at the experimental temperature of 165 °C is also indicated.

The results of the microwave studies[41,42] are in agreement with an electron diffraction study[45] and the various theoretical calculations that predict that the most stable conformer is **Ip**. In the case of conformer **II**, the microwave data indicate that this conformer has C_s symmetry with a planar heavy atom framework (i.e., **IIp**). At the highest levels of theory employed thus far,[25,27,28] the geometry-optimized structure is a C_1 symmetry conformer (**IIn**) resulting from a slight out-of-plane twist

(30) Császár, A. G. *J. Mol. Struct.* **1995**, *346*, 141−152.
(31) Ramek, M.; Momany, F. A.; Miller, D. M.; Schäfer, L. *J. Mol. Struct.* **1996**, *375*, 189−191.
(32) Fukui, K. In *Applied Quantum Chemistry, Proceedings of the Nobel Laureate Symposium on Applied Quantum Chemistry*; Smith, V. H., Jr., Schaefer, H. F., III, Morokuma, K., Eds.; Reidel: Boston, 1986; pp 1−25.
(33) Fukui, K.; Yonezawa, T.; Shingu, H. J. *J. Chem. Phys.* **1952**, *20*, 722−725.
(34) Hollebone, B. P.; Brion, C. E. Unpublished work.
(35) Debies, T. P.; Rabalais, J. W. *J. Electron Spectrosc. Relat. Phenom.* **1974**, *3*, 315−322.
(36) Cannington, P. H.; Ham, N. S. *J. Electron Spectrosc. Relat. Phenom.* **1983**, *32*, 139−151.
(37) The conformer labels are those used by Császár,[25] where **p** and **n** denote planar (C_s symmetry) and nonplanar (C_1) heavy atom frameworks, respectively.
(38) Suenram, R. D.; Lovas, F. J. *J. Mol. Spectrosc.* **1978**, *72*, 372−382.
(39) Brown, R. D.; Godfrey, P. D.; Storey, J. W. V.; Bassez, M.-P. *J. Chem. Soc., Chem. Commun.* **1978**, 547−548.
(40) Schäfer, L.; Sellers, H. L.; Lovas, F. J.; Suenram, R. D. *J. Am. Chem. Soc.* **1980**, *102*, 6566−6568.
(41) Suenram, R. D.; Lovas, F. J. *J. Am. Chem. Soc.* **1980**, *102*, 7180−7184.
(42) Godfrey, P. D.; Brown, R. D. *J. Am. Chem. Soc.* **1995**, *117*, 2019−2023.
(43) Godfrey, P. D.; Brown, R. D.; Rodgers, F. M. *J. Mol. Struct.* **1996**, *376*, 65−81.
(44) Reva, I. D.; Plokhotnichenko, A. M.; Stepanian, S. G.; Ivanov, A. Y.; Radchenko, E. D.; Sheina, G. G.; Blagoi, Y. P. *Chem. Phys. Lett.* **1995**, *232*, 141−148; Erratum. *Chem. Phys. Lett.* **1995**, *235*, 617.
(45) Iijima, K.; Tanaka, K.; Onuma, S. *J. Mol. Struct.* **1991**, *246*, 257−266.

of the planar heavy atom skeleton. These calculations also indicate that structure **IIp** is a saddle point between two equivalent **IIn** structures.[22,24,25,27] However, the energy difference between the **IIp** and **IIn** forms is calculated to be quite small and is less than the calculated zero-point vibrational energy. Therefore, while the equilibrium geometry may correspond to **IIn**, the average geometry is expected[22,23,25,27,42] to be **IIp**, in agreement with the microwave studies. In the case of the third conformer, the calculated energy minimum is either the C_s symmetry **IIIp** or the C_1 symmetry **IIIn** form, depending upon the theoretical method and basis set used. However, the highest level post-HF and DFT calculations[25,27−29] all predict **IIIp** to be the true energy minimum, although the energy difference from **IIIn** is very small (∼0.03 kJ/mol). Of the remaining predicted energy minima, three (**IVn**, **Vn**, and **VIIIn**) are of C_1 symmetry and two (**VIp** and **VIIp**) are of C_s symmetry. These C_1 symmetry conformers (**IVn**, **Vn**, and **VIIIn**) differ considerably from their C_s symmetry analogs in terms of both geometry and energy, in contrast to the situation for **IIn** and **IIIn** described above.

Experimental Methods

Details of the construction and operation of the energy dispersive multichannel electron momentum spectrometer used in the present work have been described previously.[15] In this spectrometer, gas phase target molecules are ionized by impact with a high-energy (1200 eV + binding energy) electron beam and the two outgoing electrons are angle and energy selected before being detected in coincidence. The experimental geometry, referred to as symmetric noncoplanar, is such that the two outgoing electrons are selected at equal polar angles ($\theta_1 = \theta_2 = 45°$) relative to the forward-scattered electron beam. Position sensitive detectors at the exit planes of two hemispherical electron analyzers each detect electrons over a range of kinetic energies from 596 to 604 eV. Only events where electrons arrive at each detector simultaneously and where their summed energy is in the range 1200 ± 3.5 eV are recorded.[15] The momentum of the struck electron prior to ionization is monitored by varying the relative azimuthal angle ϕ between the two analyzers. Under the binary encounter requirements[12] of high impact energy and high momentum transfer, the momentum p of the ionized electron prior to impact is related to the azimuthal angle by

$$p = [(2p_1 \cos\theta_1 - p_0)^2 + (2p_1 \sin\theta_1 \sin(\phi/2))^2]^{1/2} \qquad (1)$$

where p_0, p_1, and p_2 ($p_1 = p_2$) are the momenta of the ionizing and each of the two outgoing electrons, respectively. In the present work, binding energy spectra of gaseous glycine over the energy range of 6−27 eV were recorded sequentially at relative azimuthal angles of 0°, 1°, 2°, 3°, 4°, 6°, 8°, 11°, 14°, 17°, 20°, 25°, and 30° by scanning the energy of the incident electron beam. Many scans were accumulated over an appreciable measuring time (∼1100 h) in order to improve the signal to noise ratio. A heated sample probe[18] incorporating a glass sample holder was used to admit gaseous glycine into the experimental interaction region by sublimation of the solid sample (from MCB Chemicals) at 165 °C. Earlier experiments have shown that when glycine is sublimated in this temperature range using glass sample holders, sample decomposition does not occur.[46,47]

In EMS experiments, individual orbitals are selected for study according to their characteristic binding (ionization) energies. The variation in experimental signal (cross-section) as a function of momentum (determined from ϕ using eq 1) for a particular binding energy-selected orbital is the experimental momentum profile, or XMP, for that orbital. In the case of glycine, the Franck−Condon widths and close energy spacing of the ionization peaks necessitated the use of a fitting procedure to obtain individual orbital XMPs. The set of 13 binding energy spectra (BES) were fitted using Gaussian peaks for each ionization process located at published vertical ionization energies determined by high-resolution photoelectron spectroscopy (PES).[36] The widths of the fitted peaks were fixed at values obtained by convoluting the EMS instrumental energy resolution function (fwhm = 1.5 eV) with the Franck−Condon widths of the ionization peaks estimated by fitting Gaussian functions to the high-resolution PES spectrum reported by Cannington and Ham.[36] The distribution of fitted peak areas for an individual ionization process as a function of momentum is the desired XMP.

The experimental energy resolution function (1.5 eV fwhm) and the momentum resolution (∼0.1 au fwhm) of the spectrometer were determined from measurements of the helium $1s^{-1}$ binding energy peak and the momentum profile of the argon 3p orbital, respectively. Helium gas was admitted into the collision chamber during data acquisition for glycine to serve as an internal standard for energy calibration and to aid in the monitoring of the experimental conditions. In particular, it was necessary to ensure that no charging effects occurred on condensed glycine deposits which built up inside the spectrometer during the experiment. No change in the width or position of the sharp He $1s^{-1}$ peak was detected during the long data accumulation period.

Theoretical Methods

EMS Theory. Using symmetric noncoplanar kinematics, the EMS cross-section for randomly oriented (e.g., gas phase) molecules in the plane wave impulse approximation is proportional to the spherically averaged square of the overlap of the initial neutral molecule wave function $|\Psi_i^N\rangle$ and the final ion wave function $|\Psi_f^{N-1}\rangle$ as given by[12]

$$\sigma_{EMS} \propto \int d\Omega\, |\langle \vec{p}\Psi_f^{N-1}|\Psi_i^N\rangle|^2 \qquad (2)$$

where $\vec{p}$ refers to the momentum of the ionized electron. If the many-body wave functions $|\Psi_i^N\rangle$ and $|\Psi_i^{N-1}\rangle$ are replaced by the independent particle determinants of target Hartree−Fock orbitals (the target Hartree−Fock approximation[12]), then eq 2 simplifies to

$$\sigma_{EMS} \propto S_j^f \int d\Omega\, |\psi_j(\vec{p})|^2 \qquad (3)$$

where $\psi_j(\vec{p})$ is the momentum-space representation of the molecular orbital from which the electron was ionized and the spectroscopic factor S_j^f is the probability that the final ion state Ψ_f^{N-1} contains a hole in orbital ψ_j. Thus, within the approximations involved in eq 3, EMS provides imaging of the orbital electron density in momentum space ($|\psi_j(\vec{p})|^2$). In instances where a single particle model of ionization holds, as is typically the case for ionization from the outer-valence orbitals of molecules, the spectroscopic factor will be near unity. However, when this model starts to break down, ionization from an orbital ψ_j may occur at several ionization energies, each leading to a different final ion state Ψ_f^{N-1}. Within the target Hartree−Fock approximation, each of these ionization processes will yield an EMS cross-section having a shape characteristic of orbital ψ_j and given by eq 3. Note that the momentum space orbital $\psi_j(\vec{p})$ is the Fourier transform of the more familiar position space quantity $\psi_j(\vec{r})$.

Recently, eq 2 has been reinterpreted in the context of Kohn−Sham density functional theory.[9,48] In a manner similar to that described for the target Hartree−Fock approximation above (eq 3), the ion−neutral overlap term in eq 2 can be expressed in terms of the Kohn−Sham orbitals $\{\psi^{KS}\}$ to give the target Kohn−Sham approximation:[9,48]

$$\sigma_{EMS} \propto \int d\Omega\, |\psi_j^{KS}(\vec{p})|^2 \qquad (4)$$

The target Kohn−Sham approximation of the EMS cross-section provides for the inclusion of electron correlation and exchange in the target ground state through the exchange-correlation potential energy functional.

Computational Details. In the present work, HF and DFT calculations were performed for each of the eight MP2/6-311++G** geometry optimized conformers shown in Figure 1 and predicted by Császár[25] to be energy minima on the glycine conformational potential energy surface. Following the labeling scheme used by Császár,[25]

(46) Gross, D.; Grodsky, G. *J. Am. Chem. Soc.* **1955**, *77*, 1678−1680.
(47) Junk, G.; Svec, H. *J. Am. Chem. Soc.* **1963**, *85*, 839−845.
(48) Casida, M. E. *Phys. Rev. A* **1995**, *51*, 2005−2013.

Table 1. Computational Details and Selected Calculated Properties for Glycine

key	method	basis set: name	basis set: contracted functions [heavy atoms/H]	total energy (hartrees) **Ip**	dipole moment[a] (D): **Ip**	dipole moment[a] (D): **IIp**
st	HF	STO-3G[e]	[2s,1p/1s]	−279.114 538	1.1850	4.6378
4g	HF	4−31G[e]	[3s,2p/2s]	−282.403 960	1.2707	6.9355
6g	HF	6−311G[e]	[4s,3p/3s]	−282.768 248	1.2581	6.9138
6p	HF	6−311++G**[e]	[5s,4p,1d/4s,1p]	−282.921 717	1.2861	6.3021
tt	HF	trun-pVTZ[f]	[5s,4p,3d/4s,3p]	−282.942 077	1.2752	6.0976
tz	HF	aug-cc-pVTZ[g]	[5s,4p,3d,2f/4s,3p,2d]	−282.951 366	1.2764	6.0966
ld	DFT-LDA[b]	trun-pVTZ[f]	[5s,4p,3d/4s,3p]	−282.326 642	1.2100	5.7153
bp	DFT-BP[c]	trun-pVTZ[f]	[5s,4p,3d/4s,3p]	−284.572 595	1.1819	5.5910
b3	DFT-B3LYP[d]	trun-pVTZ[f]	[5s,4p,3d/4s,3p]	−284.548 905	1.1988	5.6892
	experiment				1.0−1.4[h]	4.5−4.6[i]

[a] Theoretical values are for a nonrotating, nonvibrating molecule. [b] The Vosko, Wilk, and Nusair[52] local exchange-correlation potential energy functional was used. [c] The Becke exchange[54] and Perdew correlation[53] gradient corrections to the exchange-correlation potential energy functional were used. [d] See ref 55. [e] Internal basis set of GAUSSIAN92.[56] [f] The trun-pVTZ basis set is the aug-cc-pVTZ basis set with the f functions on the heavy atoms and the d functions on the hydrogens removed (see ref 51). [g] From refs 49 and 50. [h] Suenram and Lovas[41] determined μ_a of conformer **Ip** to be 1.0 ± 0.15 D and $\mu_b \neq 0$, $\mu_a > \mu_b$. [i] Brown et al.[39] found μ_a of conformer **IIp** to be 4.5 D and $\mu_b < 1$ D.

Table 2. Thermodynamic Quantities for the Conformers of Glycine Calculated at the Experimental Temperature of 438 K[a]

conformer	ΔE^0 [b] (kJ/mol)	$\Delta(\Delta E^{438})$ (kJ/mol)	ΔS^{438} (J/(mol·K))	ΔG^{438} (kJ/mol)	abundance (%)	exptl energy (kJ/mol)
Ip	0.0	0.0	0.0	0.0	52.61	
IIn	2.058	0.308	−9.321	6.449	8.96	5.4−6.7,[c] 5.9 ± 1.8[d]
IIIp	6.663	0.153	10.764	2.100	29.56	3.8−6.3[c]
IVn	5.156	−0.199	−5.720	7.463	6.78	
Vn	10.503	0.026	−4.852	12.655	1.63	
VIp	19.750	−0.603	1.498	18.491	0.33	
VIIp	24.081	−1.018	0.136	23.004	0.10	
VIIIn	25.265	−0.711	−4.420	26.491	0.04	

[a] All values are relative to those for conformer **Ip**. Vibrational frequencies and rotational constants from ref 25 were used to calculate the relative entropies (ΔS) and relative thermal energies ($\Delta(\Delta E)$) for all conformers except **IIIp**, for which the vibrational frequencies from ref 27 were used. [b] Best MP estimates from ref 25. [c] Infrared spectroscopy of glycine (140−150 °C) isolated in an inert gas matrix, ref 44. [d] Microwave spectroscopy (170−180 °C), ref 41.

calculations were carried out for the C_s symmetry conformers **Ip**, **IIp**, **IIIp**, **VIp**, and **VIIp** (having a planar heavy-atom skeleton) and the C_1 symmetry conformers **IVn**, **Vn**, and **VIIIn**. The **IIp** and **IIIp** geometries were used for this study even though they are saddle points rather than energy minima on the MP2/6-311++G** potential energy surface because, as discussed in the Introduction, in both cases the effective ground state structures are expected to be the C_s symmetry conformers. The HF calculations for each of these eight conformers were performed using a series of basis sets of increasing complexity, ranging from the STO-3G (st) minimal basis set with 30 contracted Gaussian functions (CGFs) to the 345-CGF near-Hartree-Fock limit aug-cc-pVTZ (tz) basis set of Dunning and co-workers.[49,50] Theoretical EMS cross-sections for the valence orbitals of each of the conformers were obtained using eq 3 with each of the HF wave functions. Cross-sections were also calculated using eq 4 from the Kohn−Sham orbitals obtained from DFT calculations. The KS-DFT calculations were performed with a variant of the aug-cc-pVTZ basis set, referred to in the present work as the trun-pVTZ (tt) basis set, from which the heavy-atom f functions and hydrogen d functions have been removed (240-CGF).[51] The DFT calculations were performed within the local density approximation using the Vosko, Wilk, and Nusair[52] functional (ld) and also using two nonlocal functionals: the first (bp) including the Perdew correlation[53] and Becke exchange[54] gradient corrections and the second (b3) being the B3LYP hybrid functional.[55] Further computational details and selected calculated properties are shown in Table 1. All HF calculations were performed using GAUSSIAN92[56] and internal basis sets with the exception of the aug-cc-pVTZ and trun-pVTZ basis sets mentioned above. DFT calculations with the ld and bp functionals were performed using the deMon[57,58] density functional program with an "extrafine nonrandom" grid while the b3 DFT calculations were performed using GAUSSIAN92 with the "Int=FineGrid" option.

To compare the cross-sections calculated using eqs 3 and 4 above with the experimental momentum profiles, the effects of the finite spectrometer acceptance angles (i.e., the momentum resolution) in both θ and ϕ ($\Delta\theta = \pm 0.6°$ and $\Delta\phi = \pm 1.2°$) must be folded into the calculated cross-sections. This has been done in the present work using the Gaussian-weighted planar grid method of Duffy et al.[59] The theoretical cross-sections including the effects of the instrumental angular resolution are referred to as theoretical momentum profiles (TMPs).

For comparison with the experimental momentum profiles, the TMPs for the five lowest energy conformers (**Ip**, **IIp**, **IIIp**, **IVn**, and **Vn**) were Boltzmann weighted according to the experimental temperature of 165 °C and their calculated Gibbs free energies at that temperature relative to the free energy of the most stable conformer, and summed together. The remaining three conformers (**VIp**, **VIIp**, and **VIIIn**) were not included in this sum since the free energy calculations indicate that they will account for only ∼0.5% of the sample at the experimental temperature. The use of free energies for the TMP weighting is a more physically realistic treatment than the use of electronic energies alone, as was done in a preliminary analysis of the glycine HOMO electron density.[19] The calculated thermodynamic quantities are summarized in Table 2. The relative free energies at 165 °C differ significantly

(49) Dunning, Jr., T. H. *J. Chem. Phys.* **1989**, *90*, 1007−1023.
(50) Kendall, R. A.; Dunning, Jr., T. H.; Harrison, R. J. *J. Chem. Phys.* **1992**, *96*, 6796−6806.
(51) This truncation was necessary because the version of the *deMon* DFT program used cannot process f functions.
(52) Vosko, S. H.; Wilk, L.; Nusair, M. *Can. J. Phys.* **1980**, *58*, 1200−1211.
(53) Perdew, J. P. *Phys. Rev. B* **1986**, *33*, 8822−8824.
(54) Becke, A. D. *Phys. Rev. A* **1988**, *38*, 3098−3100.
(55) The B3LYP functional is a modification of the hybrid functional proposed by Becke[65] and incorporating the exact exchange energy, with the Lee, Yang, and Parr[66] correlation potential replacing that of Perdew and Wang.[67]
(56) Frisch, M. J.; et al. *Gaussian 92/DFT*, Revision F.4; Gaussian, Inc.: Pittsburgh PA, 1993.
(57) St-Amant, A.; Salahub, D. R. *Chem. Phys. Lett.* **1990**, *169*, 387−392.
(58) Salahub, D. R.; Fournier, R.; Mlanarski, P.; Papai, I.; St-Amant, A.; Ushio, J. In *Density Functional Methods in Chemistry*; Labanowski, J., Andzelm, J., Eds.; Springer-Verlag: New York, 1991; pp 77−100.
(59) Duffy, P.; Casida, M. E.; Brion, C. E.; Chong, D. P. *Chem. Phys.* **1992**, *159*, 347−363.

from the relative electronic energies of the glycine conformers. Free energies were calculated with the harmonic oscillator−rigid rotor approximation using standard statistical-mechanical formulas.[60] The final predictions of Császár[25] for the relative conformer energies were used for the relative electronic energies ΔE^0. The rotational constants and vibrational frequencies reported by Császár[25] for the MP2/6-311++G** geometry optimized conformers were then used to calculate the relative zero-point vibrational energies, thermal energies, and entropies of the conformers. The vibrational frequencies of conformer **IIIp** were not reported by Császár, so the relative thermodynamic properties for this conformer were calculated using the vibrational frequencies reported by Schaefer et al.[27] and calculated at the HF/DZP level. Relative Gibbs free energies at 438 K were then calculated using the equation

$$\Delta G^{438} = \Delta E^0 + \Delta(\Delta E^{438}) - 438\Delta S^{438} \quad (5)$$

where $\Delta E^0 + \Delta(\Delta E^{438})$ is ΔH^{438} and $\Delta(\Delta E^{438})$ consists of the relative zero-point vibrational energies and relative thermal energies. Previously reported experimentally determined energies for conformers **IIp** and **IIIp** relative to conformer **Ip** are also included in Table 2. The experimental values for **IIp** are in agreement with the calculated relative Gibbs free energy for this conformer. The disagreement between the calculated and experimental values for **IIIp** could be a result of the use of HF[27] rather than MP2[25] vibrational frequencies to calculate the free energy of this conformer[61] or uncertainties in the experimental value, determined in a challenging experiment involving infrared spectroscopy of glycine trapped in an inert gas matrix.[44]

Results

The glycine binding energy spectra obtained at relative azimuthal angles of 0° and 8° are shown in Figure 2, with the fitted Gaussian peaks used to obtain the experimental momentum profiles shown as dashed lines. The high-resolution PES spectrum, digitized from Figure 1 of ref 36, from which the vertical ionization peak positions and Franck−Condon widths used for the fitting procedure were determined, is shown in the bottom panel of Figure 2. The reported ionization potentials and fitted Gaussian functions are indicated by vertical bars and dashed lines, respectively. The absolute energy scale of the BES was established using the He $1s^{-1}$ ionization peak at 24.58 eV.

The experimental momentum profiles (XMPs) for the valence orbitals of glycine, obtained from the peaks fitted to the 13 BES, are shown in Figures 3, 4, and 6−12 (see below). Also shown in these figures are the calculated TMPs produced using the range of theoretical models discussed above. The TMPs used for comparison with the experimental data are a sum of the TMPs for the five conformers (**Ip**, **IIp**, **IIIp**, **IVn**, and **Vn**) predicted to be the most prevalent in the sample mixture (>99.5%), Boltzmann weighted according to their relative Gibbs free energies and the experimental temperature of 165 °C, as explained in the previous section. Also shown in Figures 4, 6, 7, and 10 are the individual TMPs for these five most stable conformers. Although the XMPs as measured are on a common relative intensity scale, the data are not absolute. Therefore, a single normalization between theory and experiment is necessary before the calculations and measurements may be compared. This has been done by comparing the XMP obtained by summing fitted peaks a, b, and c (ionization potentials (IPs) 10.1, 11.2, and 12.1 eV) with the corresponding b3 DFT TMP for the sum of molecular orbitals (MOs) 20−18, as shown in Figure 3. A least-squares fit of the XMP to the b3 DFT TMP was then performed since this theoretical distribution provides the best overall agreement for shape with the experimental data. All experimental profiles for glycine were then scaled using the factor resulting from this fit, with all HF and DFT theoretical profiles kept on a common intensity scale.

Discussion

Glycine is a 40-electron molecule, with 15 valence orbitals. The PES study of Cannington and Ham,[36] as well as the HF calculations performed in the present study, indicate that ionizations from the 12 highest energy valence orbitals should be observable in the energy range studied in the current work. In the case of the C_s symmetry conformers, eight of these orbitals have a′ symmetry and four have a″ symmetry. The remaining three valence and five core orbitals outside of the energy range of this study are all of a′ symmetry. By analogy with atomic orbitals, momentum profiles having a maximum at zero momentum are commonly referred to as s-type and those having a minimum at zero momentum and a maximum at some other momentum value are referred to as p-type. In the case of glycine, ionizations from the a″ symmetry orbitals of C_s symmetry conformers will result in p-type momentum profiles. As a consequence of the nodal plane in these orbitals, the corresponding momentum profiles will have no intensity at zero momentum except for the small contribution from instrumental momentum resolution effects.[59] Ionizations from a′ symmetry orbitals of the C_s symmetry conformers and from the orbitals of the C_1 symmetry conformers may give rise to either s-type or p-type momentum profiles, depending upon the nature of the orbital in question. For example, molecular orbitals that strongly resemble atomic p orbitals will have p-type momentum profiles, although because of the lack of a nodal plane in these molecular orbitals, greater intensity at zero momentum may be observed than in the case of the a″ momentum profiles.

Binding Energy Spectra. As a result of the close energy spacing of the glycine valence orbitals, it is not possible for the most part to identify individual ionization peaks in the EMS BES. However, examination of the $\phi = 0°$ and 8° BES shown in Figure 2 reveals five distinct regions. The lowest energy region, between approximately 9 and 12 eV, contains peaks due to ionization from the three outermost orbitals of glycine (MOs 20, 19, and 18). The observed intensity in this energy region is greater at $\phi = 8°$, indicating that these orbitals are predominantly p-type. This is as expected since these orbitals, centered predominantly on the nitrogen and two oxygen atoms, are largely "lone pair" in character. The second region, from approximately 12 to 16 eV, is of greater overall intensity than the first one, particularly in the case of the $\phi = 0°$ spectrum. This is because of the presence of ionizations from four orbitals (MOs 17−14, with IPs of 13.6, 14.4, 15.0, and 15.6 eV, from PES[36]) in this energy range and also because the overall symmetry of these bands is s-type, as a consequence of the predominantly σ-bonding nature of these orbitals. The third region, of comparable intensity to the second, runs from 16 to ~18.5 eV and is due to ionization from MOs 13, 12, and 11 (IPs 16.6, 16.9, and 17.6 eV).[36] The overall symmetry in this

(60) McQuarrie, D. A. *Statistical Mechanics*; Harper & Row: New York, 1976.

(61) In a recent density functional theory study of glycine,[29] Hagler et al. found that the use of vibrational frequencies calculated using the MP2 or B3LYP-DFT method rather than the HF method resulted in a significantly greater relative free energy for conformer **IIIp**. This difference was primarily attributed to a very low value for the first vibrational frequency of this conformer when calculated at the HF level of theory. The impact this has on the Boltzmann-weighted conformer sum TMPs discussed in the following sections has been investigated by setting the relative free energy of conformer **IIIp** to 12.02 kJ/mol, the value reported by Hagler et al.[29] for the temperature of 473 K (as opposed to 438 K used in the presently reported experiments) obtained using vibrational frequencies calculated at the MP2/DZP level of theory. Although this has a rather large effect on the estimated conformer abundances, particularly for conformers **Ip** and **IIIp**, the changes in the conformer sum TMPs for glycine are minor and do not alter the discussion in the remainder of this paper.

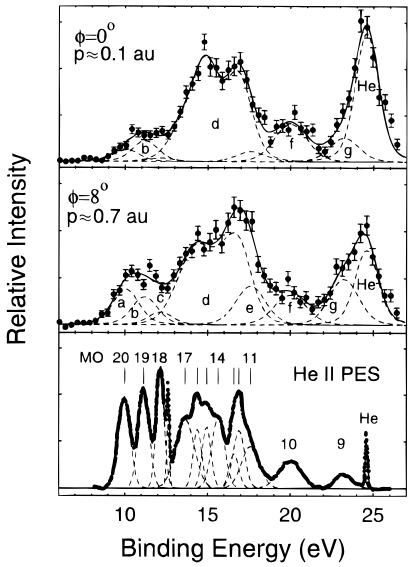

Figure 2. Binding energy spectra of glycine. The top two panels show the EMS BES from this work for the binding energy range of 6−27 eV at relative azimuthal angles of $\phi = 0°$ and 8°, obtained at an impact energy of 1200 eV + binding energy. The approximate corresponding electron momenta, calculated using eq 1, are also indicated. The dashed lines represent the result of a least-squares fit of Gaussian functions to the ionization peaks, and the solid curve is the summed fit (see the Experimental Methods for details). The areas indicated by a−g as a function of angle (momentum) give the XMPs for orbitals or sums of orbitals shown in Figures 3, 4, and 6−12. The lower panel shows the He(II) PES spectrum reported by Cannington and Ham.[36] The vertical ionization energies corresponding to the respective MOs are indicated by vertical lines. The fitted Gaussian functions used to estimate the Franck−Condon widths of the ionization processes are indicated by dashed lines. The sharp peak in the PES at 12.7 eV has been attributed by Debies and Rabalais[35] to HCl.

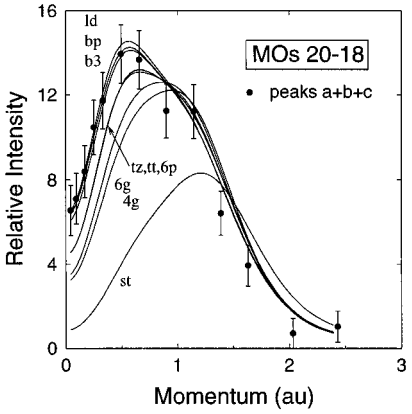

Figure 3. Experimental momentum profile for the sum of BES peaks a, b, and c (IPs 10.1, 11.2, and 12.1 eV; see Figure 2) of glycine and corresponding theoretical momentum profiles for the sum of MOs 20−18. The key to the TMP labels is given in Table 1. The XMP has been normalized to the b3 TMP.

region is p-type. The fourth "region", located at 20 eV, arises from ionization from MO 10 and is s-type, although the intensity at 8° is comparable to that at 0°. The final region in the BES shown in Figure 2 is dominated by the He $1s^{-1}$ calibration peak at 24.6 eV. However, a p-type lower energy shoulder is evident at ∼23 eV due to ionization from MO 9 of glycine.

Momentum Profiles. The momentum profile for the sum of the three outermost valence orbitals of glycine (Figure 3) exhibits p-type symmetry, as expected from the above examination of the BES. The atomic p-orbital-like nature of MOs 20, 19, and 18 results in the minimum at zero momentum. Although

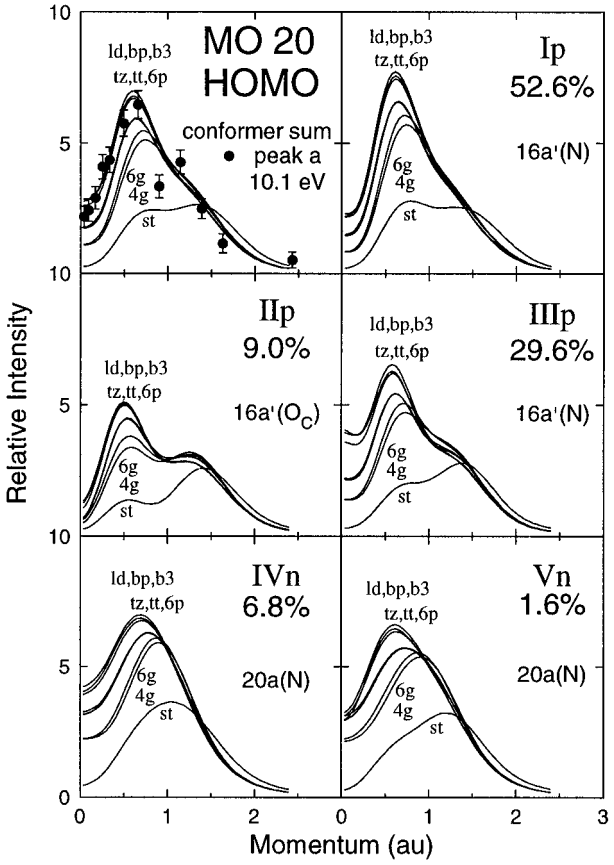

Figure 4. Experimental momentum profile for the HOMO (MO 20, IP 10.1 eV) of glycine and the corresponding theoretical momentum profiles. The XMP and the TMPs for the conformer sum are shown in the top-left panel. The remaining panels contain profiles for each of the five most abundant conformers, as indicated. The corresponding MO symmetry labels are indicated in each panel, along with the atom on which the greatest proportion of the electron density for that MO is centered. The key to the TMP labels is given in Table 1.

all of the theoretical profiles correctly predict the general shape of the experimental profile, only the DFT results (ld, bp, and b3) are in good quantitative agreement with the experimental data. The HF calculations predict the profile maximum to occur at a higher momentum than is found experimentally for these orbitals and also underestimates the intensity in the low momentum region. Not surprisingly, the discrepancy between the HF TMPs and the XMP is greatest for the 30-CGF minimal basis set calculation (st) and decreases as the basis set size increases. However, there are no significant differences between the 145-CGF 6p TMP and the 345-CGF tz TMP, suggesting that no further improvement in the agreement between the HF TMPs and experiment would be obtained by using a yet larger basis set. Although the calculated momentum profile, which emphasizes the small *p* (predominantly large *r*) region of electron density, appears converged at the HF level using the 6p basis set, further improvements in the total energy and dipole moments (see Table 1), which emphasize small and medium *r*, respectively, are obtained using the larger tt and tz basis sets. This demonstrates the importance of considering a number of properties emphasizing different regions of electron density when the accuracy of a wave function is evaluated.

The highest occupied molecular orbital of glycine, MO 20, has a binding energy of 10.1 eV as determined by EMS and a p-type momentum profile (Figure 4). The theoretical calculations indicate that this orbital is predominantly centered on the nitrogen atom and, in the case of the C_s symmetry conformers, is symmetric with respect to reflection through the plane of the

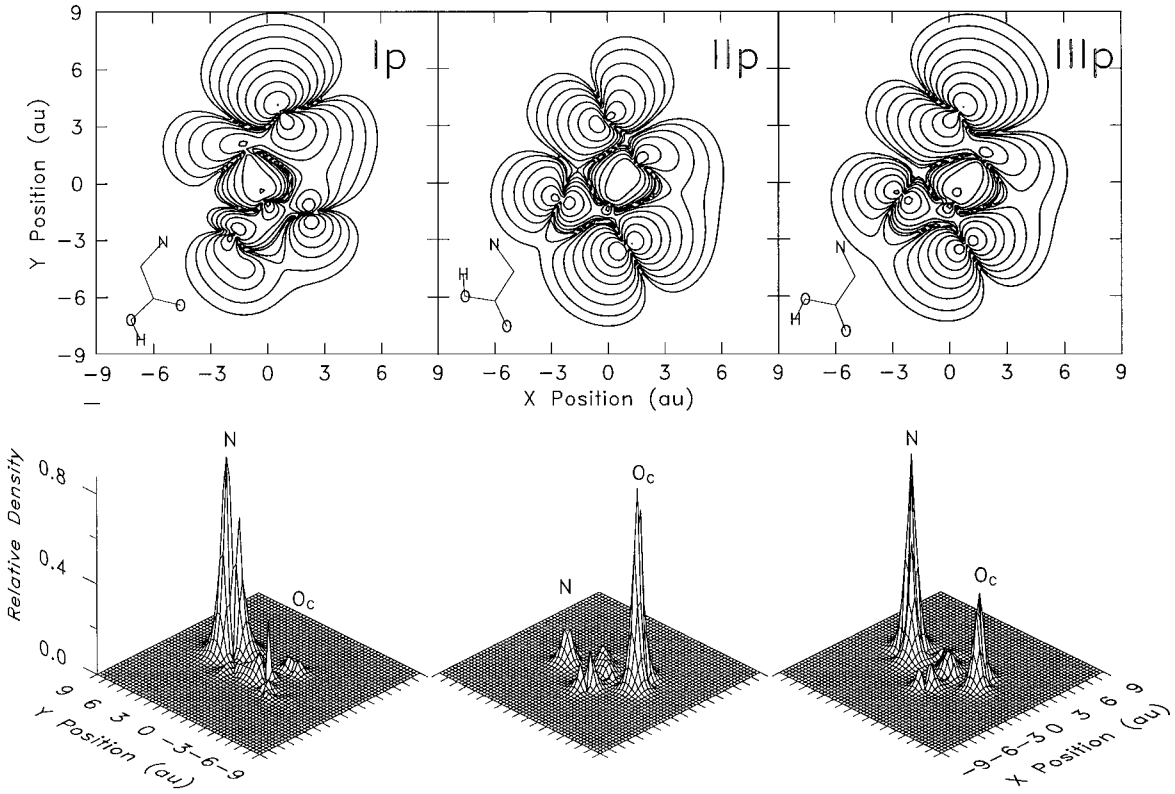

Figure 5. Position−space electron density maps for the HOMOs of the three lowest energy conformers of glycine. The maps were calculated using the results of the b3 DFT calculation. The electron density in the symmetry plane of the molecule is shown. The contour lines in the upper panels represent 0.01, 0.03, 0.1, 0.3, 1.0, 3.0, 10.0, 30.0, and 99.0% of the maximum density.

heavy-atom framework (i.e., of a′ symmetry). Note that this agrees with the PES assignment of Cannington and Ham,[36] but not the earlier assignment by Debies and Rabalais.[35] The exception is the **IIp** conformer, for which the HOMO electron density is predominantly located on the carbonyl oxygen (indicated by O_C in Figure 4). This is illustrated by the position−space electron density maps for this orbital for conformers **Ip**, **IIp**, and **IIIp**, shown in Figure 5. This difference in the nature of the HOMO is most likely a result of conformer **IIp** being the only one of the five most stable glycine conformers containing an intramolecular hydrogen bond to the nitrogen atom (see Figure 1). This will stabilize the nitrogen lone pair electron density and consequently increase the binding energy of the electrons in this orbital. Concurrently, the carbonyl oxygen nonbonding orbital of conformer **IIp** is destabilized by the unfavorable anti orientation of the acid group. The minimum in the experimental profile at zero momentum results from the nodal surface between the two lobes of electron density in this largely atomic p-like orbital. The intensity that is observed at zero momentum results from the small contributions to this orbital from electron density at other parts of the molecule, such as the σ-bonding character between the two carbon atoms evident from the electron density maps in Figure 5. The three DFT TMPs (ld, bp, and b3) provide the best agreement with the experimental data. The higher level HF TMPs (tz, tt, and 6p) are essentially indistinguishable from one another and in fair agreement with the XMP, correctly predicting the position of the profile maximum (p_{MAX}), but underestimating the intensity at low momentum. The smaller basis set HF calculations, in contrast, differ markedly from the experimental data. The 6g and 4g calculations correctly predict the qualitative shape of the momentum profile but place p_{MAX} at too great a momentum. The minimal basis set st profile fails to get even the qualitative features of the momentum profile correct. Because of this poor agreement, the 4g and st TMPs have not been included for comparison with the other XMPs of glycine in the present work. Note that the use in the present work of free energies for the Boltzmann weighting of the TMPs together with the determination of the XMP by fitting the BES has resulted in further improved agreement between the HOMO XMP and the DFT TMPs compared with the earlier preliminary analysis.[19] In this earlier analysis, the XMP was obtained by summing the experimental data over a range of binding energies, and electronic energies (rather than free energies) were used for the Boltzmann weighting of the TMPs.

Molecular orbitals 19 and 18 (Figures 6 and 7) have binding energies of 11.2 and 12.1 eV, respectively. While both may generally be described as p-type profiles, the MO 19 profile has considerably more intensity at zero momentum than does the profile for MO 18. There is some disagreement among the theoretical calculations as to the symmetries of these orbitals. In the case of conformers **Ip**, **IVn**, and **Vn**, all calculations performed predict MOs 19 and 18 to be predominantly oxygen lone pair orbitals centered on the carbonyl oxygen (O_C) and on both the carbonyl and hydroxyl oxygens (O_C, O_H), respectively. In the case of conformer **IIIp**, the DFT calculations predict MO 19 to be predominantly centered on the carbonyl oxygen and of a′ symmetry and MO 18 to be centered on both oxygen atoms and of a″ symmetry, with the situation reversed for the HF calculations. For conformer **IIp**, the ld and bp DFT results predict the electron density of MO 19 to be predominantly located on the nitrogen atom and of a′ symmetry and that of MO 18 to be concentrated on the two oxygen atoms and of a″ symmetry. The reverse is true for the HF and b3 DFT calculations. A comparison of the two XMPs and the various TMPs helps to clarify the situation. The XMP obtained at 11.2 eV (MO 19) has significant intensity at zero momentum while the 12.1 eV XMP (MO 18) essentially drops to zero near zero momentum. This drop to zero is consistent with the a″ symmetry momentum profiles, which have no intensity at zero

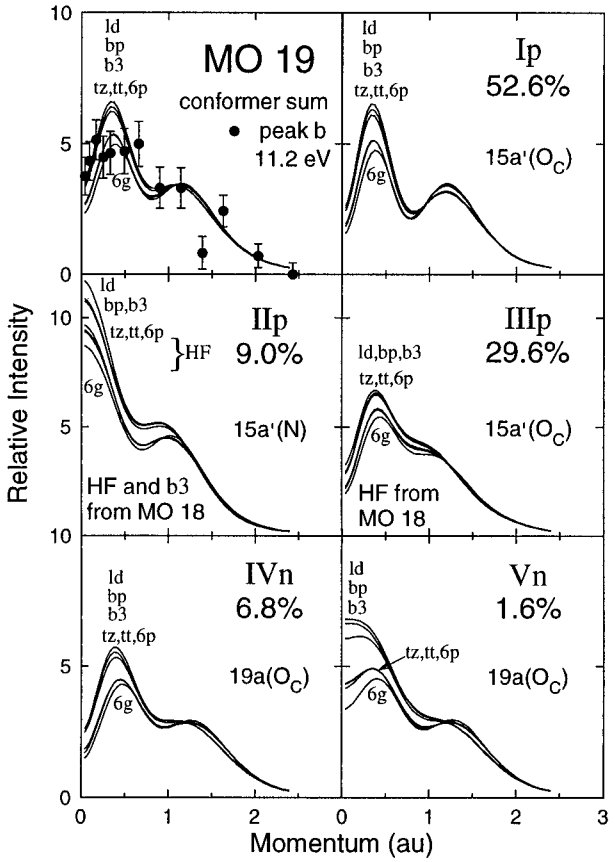

Figure 6. Experimental momentum profile for MO 19 (IP 11.2 eV) of glycine and the corresponding theoretical momentum profiles. The XMP and the TMPs for the conformer sum are shown in the top-left panel. The remaining panels contain profiles for each of the five most abundant conformers, as indicated. The corresponding MO symmetry labels are indicated in each panel, along with the atom on which the greatest proportion of the electron density for that MO is centered. The key to the TMP labels is given in Table 1.

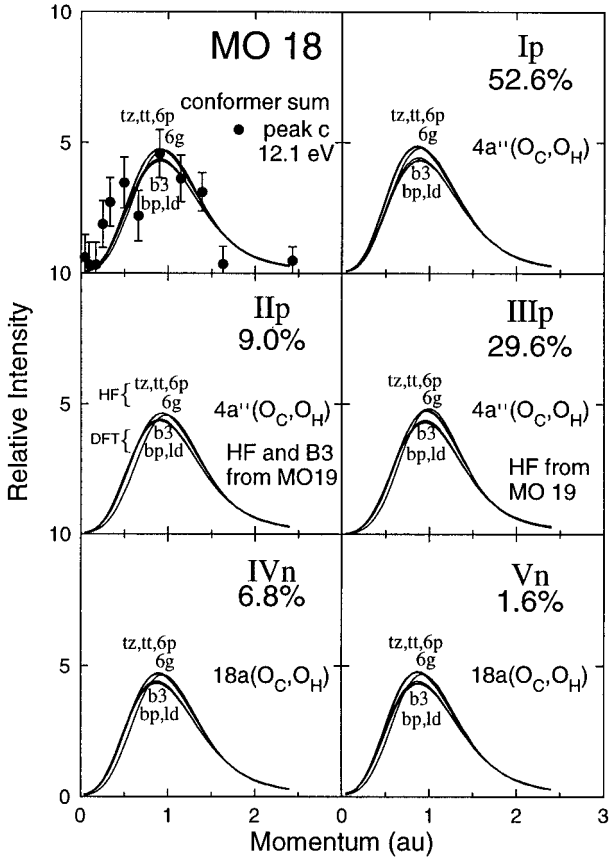

Figure 7. Experimental momentum profile for MO 18 (IP 12.1 eV) of glycine and the corresponding theoretical momentum profiles. The XMP and the TMPs for the conformer sum are shown in the top-left panel. The remaining panels contain profiles for each of the five most abundant conformers, as indicated. The corresponding MO symmetry labels are indicated in each panel, along with the atoms on which the greatest proportion of the electron density for that MO is centered. The key to the TMP labels is given in Table 1.

momentum due to the nodal plane in these orbitals. In contrast, the a′ symmetry profiles for conformers **IIp** and **IIIp** have some intensity at zero momentum. Therefore, for conformers **IIp** and **IIIp**, MO 19 may be assigned as an a′ symmetry orbital and MO 18 as an a″ symmetry orbital. This symmetry assignment is consistent with that of Cannington and Ham from a consideration of the PES of glycine and related molecules.[36] In Figures 6 and 7, the inverse ordering of orbitals 19 and 18 for conformers **IIp** and **IIIp** has been corrected as indicated to allow a more meaningful comparison of the theoretical and experimental momentum profiles. Reasonable overall shape agreement between the XMP and TMPs for each of MOs 19 and 18 is obtained. However, a comparison of the XMPs for these orbitals reveals a correspondence between some experimental data points which are lower than the theoretical profiles in the one case and higher in the other (consider in particular the points between 0.3 and 0.7 au). This is most likely a result of limitations in the energy resolution (1.5 eV) and the resulting uncertainties in the deconvolution procedure used to obtain experimental momentum profiles for these energetically closely spaced orbitals. In addition to the challenge of separating two momentum profiles differing in binding energy by only 0.9 eV, the situation for glycine is complicated by the fact that the energies for particular molecular orbitals vary to at least some degree with changes in molecular conformation. The HF/aug-cc-pVTZ calculations conducted in the present study indicate variations in orbital energy among conformers **Ip** through **Vn** of approximately 0.5 eV for each of MOs 19 and 18 and, in the

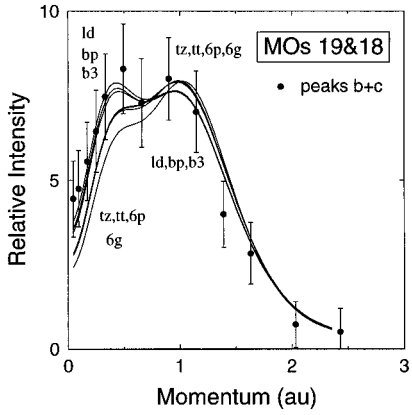

Figure 8. Experimental and theoretical momentum profiles for the sum of MOs 19 and 18 of glycine. The key to the TMP labels is given in Table 1.

case of some conformers, an energy spacing between MOs 19 and 18 of considerably less than 0.9 eV. However, a sufficient gap is predicted between the highest energy MO 20 and the lowest energy MO 19 and likewise between MOs 18 and 17 to provide reasonable confidence that a sum of fitted peaks b and c will account for all intensity due to ionization from MOs 19 and 18 without introducing intensity resulting from ionization from MO 20 or 17. In Figure 8, the XMP obtained by summing these two experimental profiles is compared with the corresponding TMPs for the sum of MOs 19 and 18. The resultant

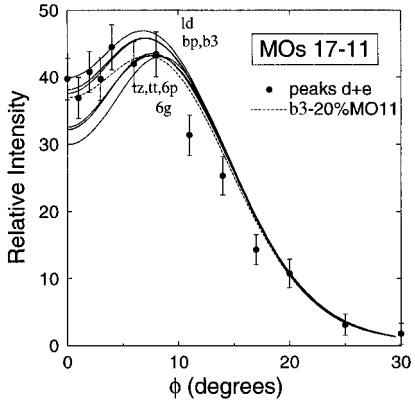

Figure 9. Experimental and theoretical angle profiles for the sum of MOs 17−11 of glycine. The key to the TMP labels is given in Table 1. The dashed line represents the b3 DFT TMP sum for MOs 17−11 minus 20% of the b3 profile for MO 11 (see the text for details).

XMP is in good quantitative shape agreement with the three DFT TMPs. In contrast, the HF TMPs give a poor representation of the experimental data in the low momentum region below p=0.7 au.

In the case of molecular orbitals 17−12 (binding energy range ~13−17 eV), the energy separation between orbitals is quite small and prevents the determination of meaningful momentum profiles for individual orbitals. For this reason, a sum of fitted peaks has been considered in this region and is compared in Figure 9 with theoretical profiles for the sum of MOs 17−11. MO 11 has also been included in the sum to avoid complications resulting from differing predictions of orbital ordering by the HF and DFT calculations. This issue is addressed further below for MO 11. The data are plotted using a relative azimuthal angle (ϕ) rather than momentum scale due to the variation of momentum with electron binding energy for a given azimuthal angle (eq 1). These orbitals are responsible for the bulk of the molecular bonding in glycine, and the σ-bonding nature of several of them results in the considerable intensity observed in the profiles at low values of ϕ. Only qualitative agreement is obtained between the shapes of the experimental profile and all of the theoretical profiles. The DFT profiles are consistent with the experimental data at small and large values of ϕ, but are higher than the experimental results for intermediate angles. The HF calculations, in contrast, fall below the experimental data at low ϕ and agree at intermediate and high values. In view of the good agreement between the DFT TMPs and the experimental data for MOs 20−18, a likely explanation for the behavior observed for MOs 17−11 is that one or more of the ionization processes occurring in this region have spectroscopic factors of less than 1 (see eq 3). If 20% of the pole strength for MO 11 is removed from the b3 DFT TMP sum for MOs 17−11, the resulting dotted line (Figure 9) shows somewhat improved agreement with experiment (see the following paragraph and Figure 10 below, where the remaining 80% of the MO 11 b3 DFT TMP fits the XMP for MO 11 quite well). It is well known that inner valence ionization processes frequently show a range of energy poles due to final ion state electron correlation effects.[62]

Experimental and theoretical momentum profiles for the ionization process at 17.6 eV, arising from ionization from MO 11, are shown in Figure 10. There is disagreement between the HF and DFT calculations as to the symmetry of this orbital. However, a comparison of the shape of the XMP with those of the various TMPs clearly indicates that, in the case of the C_s symmetry conformers, this is an a″ orbital, in agreement with the DFT predictions. An examination of the MO calculations indicates that this orbital may be primarily thought of as a pseudo-π orbital responsible for NH_2 σ-bonding, but with significant contributions to CH_2 bonding as well. For comparison between theory and experiment, the TMPs for the HF orbitals having the appropriate a″ symmetry are shown in Figure 10 (i.e., MO 13 for **Ip** and MO 12 for **IIp** and **IIIp**). Although there are also clear differences between the HF and DFT TMPs for the C_1 conformers **IVn** and **Vn**, the lack of symmetry in these conformers makes it difficult to determine the correct MOs to use for comparison with the XMP. Consequently, the predicted MO 11 TMPs have been used. Because of the small relative populations of conformers **IVn** and **Vn**, this will not significantly affect the Boltzmann-weighted conformer sum TMPs that are compared with experiment in the upper-left panel of Figure 10. It is evident from Figure 10 that there are only slight differences between calculations for this orbital and that all TMPs shown are consistent with the shape of the XMP. There is, however, a considerable discrepancy in terms of intensity between theory and experiment. The b3 TMP must be scaled by 80% to bring it into agreement with the XMP. This represents a breakdown of the single particle model of ionization due to final state correlation and relaxation effects. The missing 20% intensity would be expected to be observed as satellite peaks at other binding energies, possibly outside of the energy range examined in the current study. This "missing intensity" at least partly explains the disagreement between theory and

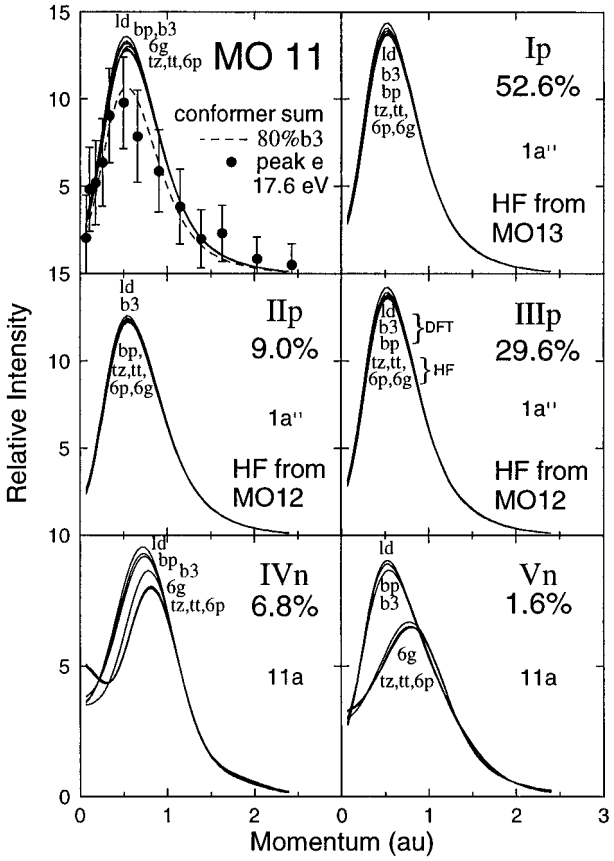

Figure 10. Experimental momentum profile for MO 11 (IP 17.6 eV) of glycine and the corresponding theoretical momentum profiles. The XMP and the TMPs for the conformer sum are shown in the top-left panel. The remaining panels contain profiles for each of the five most abundant conformers indicated. The corresponding MO symmetry labels are indicated in each panel. The key to the TMP labels is given in Table 1. The dashed line represents 80% of the b3 DFT TMP (see the text for details).

(62) von Niessen, W.; Schirmer, J.; Cederbaum, L. S. *Comput. Phys. Rep.* **1984**, *1*, 57−126.

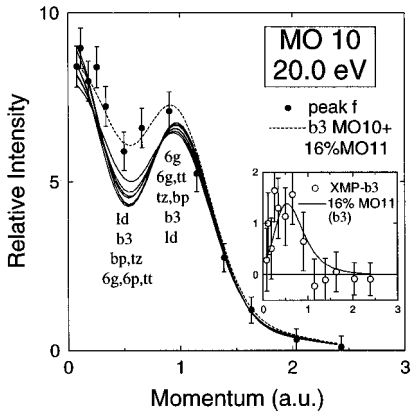

Figure 11. Experimental momentum profile for MO 10 (IP 20.0 eV) of glycine and the corresponding conformer sum theoretical momentum profiles. The key to the TMP labels is given in Table 1. The dashed line represents the b3 DFT TMP sum (MO 10 + 16% MO 11). The inset shows the XMP − b3 TMP difference (open circles) compared with 16% of the b3 TMP for MO 11.

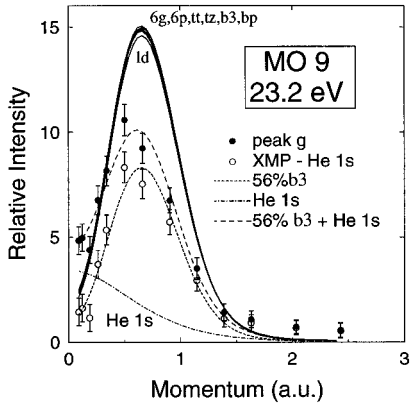

Figure 12. Experimental momentum profile for MO 9 (IP 23.2 eV) of glycine and the corresponding conformer sum theoretical momentum profiles. The key to the TMP labels is given in Table 1. The dotted−dashed line corresponds to the shape of the He 1s TMP obtained using the highly correlated He wave function reported by Davidson.[63] The short dashed line represents 56% of the b3 DFT TMP for MO 9. The long dashed line is the sum of the dotted−dashed and short dashed lines. The open circles are the result of subtracting the He 1s TMP (dotted−dashed line) from the measured XMP.

experiment seen for the sum of MOs 17−11 in Figure 9 at intermediate relative azimuthal angles (see above discussion). The shape of the MO 11 momentum profile would result in a significant drop in experimental intensity for the MO 17−11 sum at intermediate angles, but very little change at lower or higher angles if the spectroscopic factor for this ionization process at 17.6 eV is lower than unity.

In the case of MO 10 (Figure 11, electron binding energy 20.0 eV), all theoretical momentum profiles are in reasonably close agreement, differing, however, in the relative magnitudes of the maximum at 0 au and the minimum near 0.5 au. All HF and DFT calculations indicate that MO 10 consists primarily of carbon 2s electron density. However, there is also a significant σ-bonding component, particularly between the hydroxyl oxygen and hydrogen. The XMP is consistent with the general features of the theoretical profiles, although there is a significant difference in intensity for the region between approximately 0.2 and 1.0 au. One possible explanation for this additional experimentally observed intensity is the presence in this binding energy region of satellite peaks from the MO 11 ionization process (see discussion in previous paragraph and Figure 10). An examination of the momentum profile obtained by subtracting the b3 TMP for MO 10 from the 20.0 eV XMP (see inset of Figure 11) supports this explanation. The resulting profile is consistent with the b3 MO 11 TMP scaled by 16%. Including this additional intensity in the b3 TMP (dashed line, Figure 11) eliminates the discrepancy between theory and experiment.

Molecular orbital calculations indicate that MO 9, like MO 10, is comprised to a considerable degree by carbon 2s electron density. However, the two orbitals differ in that MO 9 also contains significant nitrogen 2s density and no appreciable bonding character. Upon examination of the XMP for this inner valence orbital (Figure 12), it is apparent that the spectroscopic factor for this ionization process must be significantly less than 1. In addition to this intensity difference between theory and experiment, the XMP (solid circles) is higher than all of the TMPs near zero momentum and appears to peak at a slightly lower momentum than do the TMPs. These last two observations could be a result of some contamination of this XMP with signal from the adjacent and considerably more intense s-type He $1s^{-1}$ ionization calibration peak (see Figure 2). This seems likely since, as shown in Figure 12, the XMP (solid circles) minus the scaled He 1s TMP[63] gives a momentum profile (open circles) which fits well to the b3 DFT TMP scaled by 56%.

Conclusions

The present study of glycine has demonstrated the feasibility of obtaining gas-phase experimental momentum profiles for valence orbitals of low vapor pressure solids such as amino acids which exist as a mixture of conformers. In addition, the range of targets that have been investigated by EMS has been extended to include a molecule of greater size and complexity than would have been feasible to study using single channel EMS spectrometers. A joint consideration of the experimental and theoretical results has allowed for the determination of the nature and ordering of many of the valence orbitals of glycine.

In comparing the various theoretical profiles with the experimental data, it was found that the profiles for the chemically important outer valence orbitals (MOs 20−18) are most sensitive to changes in the basis set or theoretical method used and those for MOs 11−9 are relatively insensitive to changes in the computational method. There is a steady improvement in the agreement between the HF TMPs and the XMPs with increasing basis set size. The minimal basis set STO-3G HF calculations (st in Figures 3 and 4) produce TMPs that differ dramatically from the experimental profiles. This basis set clearly does not have the necessary flexibility to accurately describe the outer valence molecular orbitals of glycine. Some improvement occurs in going to the 4-31G (4g) and 6-311G (6g) split-valence basis sets. However, the outer valence TMPs calculated using these basis sets still tend to agree poorly with the XMPs, particularly at low momentum. The addition of diffuse and polarization functions to the 6-311G basis set (the 6-311++G** (6p) calculations) results in improved agreement between theory and experiment for many of the orbitals. This is typified by an increase in the predicted intensity at low momentum and a shift of the maxima of the momentum profiles (p_{MAX}) toward zero momentum in the case of p-type profiles. This is a consequence of the improved description of the spatially diffuse regions of the electron density when using the 6-311++G** basis set. Because of the Fourier transform relationship between position and momentum

(63) Davidson, E. R. *Int. J. Quantum Chem.* **1990**, *37*, 811−819.

space, these outer regions of electron density roughly correspond to the low momentum regions in momentum space. Further increases in basis set size from the 145-CGF 6-311++G** basis set to the 240-CGF trun-pVTZ (tt) and 345-CGF aug-cc-pVTZ (tz) basis sets result in no further appreciable change in the momentum profiles. It would therefore appear unnecessary to employ such large basis sets for Hartree−Fock calculations of momentum profiles and perhaps other properties of glycine that are predominantly dependent on the "large-*r* " regions of the electron density. It is important to note, however, that further improvements in both total energy and dipole moment were obtained by using the two larger basis sets (see Table 1).

The apparent near convergence of the HF results for momentum profile, total energy, and dipole moment suggests that the HF limit has been closely approached. However, a discrepancy still remains between these theoretical profiles and the experimental data, particularly in the region of low momentum where the HF results tend to underestimate the intensity. This discrepancy is essentially removed when the KS-DFT profiles are considered. The DFT calculations predict a further shift toward low momentum in the maxima of the p-type momentum profiles from those predicted by the HF calculations. The orbital ordering predicted by the DFT calculations also appears to be more consistent with the experimental data than that predicted by the HF calculations. The improved agreement between theory and experiment, particularly at lower momentum (<1 au), can be attributed to the inclusion of electron correlation effects via the exchange-correlation potential energy functional in DFT. Although there are small differences in the momentum profiles obtained from the DFT calculations using different potential energy functionals, it is not evident that one calculation provides markedly better agreement with experiment. However, it is important to note that a recent theoretical study of the geometries and relative energies of the conformers of glycine determined using DFT found that, among the functionals considered, only the hybrid B3LYP functional reproduced the energetic ordering of the glycine conformers predicted in studies using post-HF methods.[28]

The discrepancies between even the large basis set HF calculations and the experimental momentum profile data indicate the inadequacy of noncorrelated methods for calculating the outer spatial regions of the valence orbital electron distributions of glycine, and this finding is consistent with the observation that some accounting of electron correlation is necessary for the accurate calculation of other properties (e.g., relative conformer energies) of glycine.[26] The reasonable agreement between the KS-DFT momentum profiles and the experimental data for glycine suggests that DFT is an effective choice for accounting for these electron correlation effects and modeling the longer range electron density.[64] It is of interest to note that similar results have been found for the HOMO of NH_3 by comparing EMS measurements with calculations using MRSD-CI[6,7] and also DFT[34] methods.

The importance of accounting for electron correlation effects and using relatively large, diffuse basis sets when momentum profiles are calculated for glycine suggests that this may also be necessary for other large-*r* properties of glycine and for other amino acids and proteins. If this is the case, the size of the molecule for which it will be feasible to perform accurate calculations will be quite restricted using post-HF theoretical methods. For this reason, the success of the less computationally intensive DFT in the current work is particularly encouraging. The current work indicates that in particular the long-range outer spatial regions of the electron density in the frontier orbitals of glycine are more adequately described when correlation effects are included. This may prove important for problems of modeling reactivity, molecular recognition, and molecular similarity involving amino acids and proteins in computer-aided molecular design.

Acknowledgment. This project received financial support from The Canadian National Networks of Centres of Excellence Program—Centre of Excellence in Molecular and Interfacial Dynamics (CEMAID) and also from The Natural Sciences and Engineering Research Council of Canada (NSERC). We greatfully acknowledge D. R. Salahub for providing us with a copy of ref 29 prior to publication. J.J.N. gratefully acknowledges the receipt of an NSERC postgraduate scholarship.

JA9613015

(64) Note that for extremely long range regions of electron density, currently available functionals are in error as a consequence of their incorrect asymptotic forms.

(65) Becke, A. D. *J. Chem. Phys.* **1993**, *98*, 5648−5652.
(66) Lee, C.; Yang, W.; Parr, R. G. *Phys. Rev. B* **1988**, *37*, 785−789.
(67) Perdew, J. P.; Wang, Y. *Phys. Rev. B* **1992**, *45*, 13244−13249.